INFLUENCE OF LITHIUM CONTENT ON THE STRUCTURE AND IONIC CONDUCTIVITY OF PEROVSKITE La$_{(2/3)-x}$Li$_{3x}$TiO$_3$ MADE BY DOUBLE MECHANICAL ALLOYING METHOD

LE DINH TRONG
Hanoi Pedagogical University No.2

E-mail: trongldsp2@gmail.com

Abstract. *Perovskite La$_{(2/3)-x}$Li$_{3x}$TiO$_3$ samples with $0.06 \leqslant x \leqslant 0.15$ were prepared by a double mechanical alloying method. Structure and Li$^+$-ion conductive properties of the La$_{(2/3)-x}$Li$_{3x}$TiO$_3$ samples were investigated. Most of the analyzed perovskite samples exhibit a double unit cell. In these samples, a change of symmetry from tetragonal to orthorhombic is observed for sample with lithium content x = 0.06. Structural modifications were obtained mainly due to the cation vacancies ordering along the c-axis, which disappeared gradually when the lithium content increased. At room temperature, the maximum values of grains and grain boundaries conductivities of the La$_{(2/3)-x}$Li$_{3x}$TiO$_3$ samples were found to be of 1.5×10^{-3} S/cm and 5.8×10^{-5} S/cm, respectively. The temperature dependence of ionic conductivity obeyed a non-Arrhenius behaviour. At temperature from 30 to 125 ^{o}C, the activation energy for grain and grain-boundary conductivity was found to be of $\sim$ 0.23 eV and $\sim$ 0.32 eV, respectively.*

Keywords: double mechanical alloying; perovskite structure; lithium onic conductivity, impedance spectra.

I. INTRODUCTION

Recently, ionic conducting solid materials have received considerable attention due to their potential applications in all-solid-state ionic batteries, energy storage and conversion, electrochromic displays, and in environmental monitoring electrochemical sensors, etc [1]. These materials are non-toxic solid electrolytes exhibiting easy preservation and comfortable use. From many works it is seen that a family of the perovskite structure of La$_{(2/3)-x}$Li$_{3x}$TiO$_3$ (hereafter abbreviated to LLTO) possess the best lithium ionic conductor. At room temperature, their grain conductivity can reach a value up to 10^{-3} S.cm^{-1} [2-7]. However, the grain-boundary conductivity is still low and strongly dependent on conditions of samples preparation. This results in the deacrease of the total conductivity of polycrystalline LLTO materials (namely 10^{-5} S.cm^{-1}).

In fact, the polycrystalline materials are used for most practical applications, thus the effect of the grain-boundary must be taken into account to determine the ionic conduction. In recent years, to enhance the Li$^+$ ion conductivity, great efforts have been devoted to analyzing structural and other intrinsic attributes of the LLTO, such as the concentrations of charge carriers and vacancies [3,4,6] lithium coordination [8], structural distortions [6,9], vacant site distribution [8,10,11],

charge carrier mobility [12], etc. Using the extended synchrotron X-ray absorption fine structure (EXAFS) analysis, the author in [13] demonstrated that the lithium ion conductivity is governed by main two factors: (i) the Coulombic repulsion force between the lithium ion and the titanium ion and; (ii) the bottle-neck distortion in the lithium ion channels consisted of four oxygen ions. Previous works also showed that the electrical performance of LLTO ceramics is strongly dependent on their chemical homogeneity, particle size and morphology of initial LLTO powders. Thus the synthesis of LLTO powders always plays an important role in getting LLTO ceramics with desired properties [14, 15].

In recent previous work [7], we reported on annealing effect on the Li^+ ionic conductivity of perovskite $La_{(2/3)x}Li_{3x}TiO_3$ prepared by a double mechanical alloying (dMA) method. The results showed that $1200\,°C$ is an optimal temperature for sintering LLTO with a high total conductivity. In this work, the composition dependence of the on the crystal structure and electrical properties of LLTO samples has been studied. X-ray difraction (XRD), Raman scattering (RSS) and electrical impedance spectra (IS) of the LLTO ceramics with different Li contents have been presented.

II. EXPERIMENTAL

$La_{(2/3)-x}Li_{3x}TiO_3$ crystalline powders ($0.06 \leqslant x \leqslant 0.15$) were prepared from the stoichiometric mixture of dehydrated La_2O_3 (99.9%), Li_2CO_3 (99.9%) and TiO_2 (99.8%) powders which were purchased from Aldrich Ltd. The solid state reaction of the LLTO formation is as follows:

$$((2/3) - x)La_2O_3 + 3xLi_2CO_3 + 2TiO_2 \rightarrow 2La_{(2/3)-x}Li_{3x}TiO_3 + 3xCO_2. \tag{1}$$
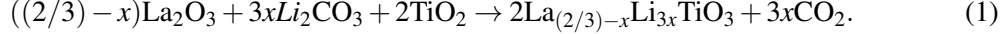
where seven values of "x" were chosen as 0.06, 0.09, 0.10, 0.11, 0.12, 0.13 and 0.15. Samples corresponding to these compounds are called LLTO06, LLTO09, LLTO10, LLTO11, LLTO12, LLTO13 and LLTO15, respectively.

By dMA method, the LLTO powder synthesized according to the following procedure. The initial materials, including La_2O_3, Li_2CO_3 and TiO_2 were mixed and grinded with absolute alcohol for 4 h, by a grinder of "Fritsch model Pulverisette 6". The cation molar ratio in the samples is La:Li:Ti = ((2/3)-x):3x:1. The grinded mixture is dried at 200 ^{o}C, then preliminarily annealed at 800 $°C$ in air, for 4 h in order to eliminate CO_2. Afterwards, the mixtures were react-grinded by a grinder at speed of 600 rev/min for 6 h. The obtained powder was referred to the "precursor" hereafter. To prepare ceramic specimens, precursor powder was isostatically pressed under $\sim$450 MPa into pellets with 12.5 mm in diameter and 1.5 mm in thickness. Finally, the pellets were sintered at temperatures 1200°C for 4 h with a heating rate of 5 ^{o}C/minand the cooling is natural.

Phase purity and crystalline structure of the obtained materials were determined by XRD analysis on a Siemen D5000 diffractometer, at room temperature using CuKα radiation. To research the molecular structure of the sample LLTO, the RSS was done on "LABRAM-1B" Micro-Raman spectrometer. Equipment used excitation radiation source is He-Ne laser has a wavelength of 632.8 nm, the backscattering configuration.

The ionic conduction properties of all samples were characterized by IS analysis on AutoLab. Potentiostat-PGS30 using FRA-2 impedance software. To characterize impedance spectroscopy (IS) the samples were mechanically polished and chemically treated in order to have clean and parallel surfaces, then on these surfaces a metallic silver coating with 8 mm-diameter circle was vacuum evaporated. Thus, two silver parallel electrodes of an area of A $\approx$ 0.5 cm^2

were used for electrical measurements. IS measurements were recorded under normal atmosphere between room temperature (RT) and 200 ^oC, in the frequency range of 0.1 to 10^6 Hz with an amplitude of 20 mV. The grain and grain boundary resistances of the samples were obtained by fitting experimental data with the theoretical curves using appropriate equivalent schema, as has been shown in previous reports [7].

III. RESULTS AND DISCUSSION

III.1. Crystalline structure

The powder XRD patterns of the react-grinded samples are presented in Fig. 1. All main diffraction peaks are excellent fit with those reported in a literature (JCPDS 46-0465). After react-grinding, single phase structure of LLTO compounds were obtained.

The fact that XRD patterns showed rather small and broad peaks prove the uniform distribution of the nanostructured LLTO compound. Using Sherrer's formula

$$\tau = \frac{0.9\lambda}{\beta.\cos\theta}, \qquad (2)$$

an average size of the crystalline grains in the LLTO samples was found to be of about 10 nm.

Fig. 2 shows the powder X-ray diffraction (XRD) patterns of as-sintered LLTO with $x = 0.06$, $x = 0.11$ and $x = 0.15$. Three differences between the patterns can be obtained depending on the lithium content of these perovskites:

i) The shift of the diffraction peaks toward larger 2θ angle for samples with high lithium content was observed. This proves unit cell parameters decrease when replacing the lithium content increases. Calculation results received, the unit cell parameters of the LLTO06 sample are a $\approx$ 3.8659 Å, b $\approx$ 3.8771 Å, c $\approx$ 7.7726 Å down a $\approx$ 3.8634 Å, b $\approx$ 3.8747 Å, c $\approx$ 7.7649 Å for LLTO15 sample.

ii) The X-ray diffraction showed that the structure of the sample (with x = 0.6 to 0.15) are tetragonal structure with space group P4/mmm. In these samples, The superstructure
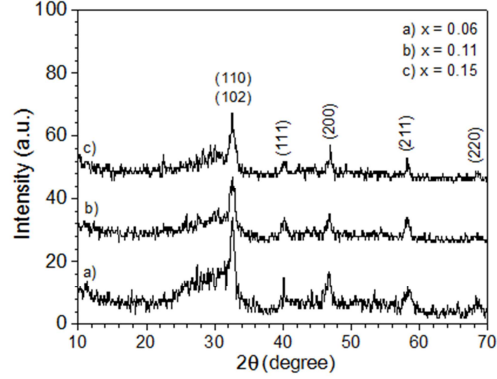
Fig. 1. Powder XRD patterns of as-react-grinded $La_{2/3-x}Li_{3x}TiO_3$ samples: a) LLTO06; b) LLTO11 and c) LLTO15.
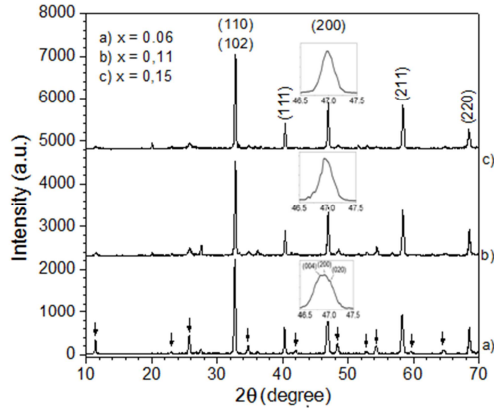
Fig. 2. Powder XRD patterns of $La_{(2/3)-x}Li_{3x}TiO_3$ perovskites for three different compositions: $x = 0.06$, $x = 0.11$ and $x = 0.15$. Superstructure peaks corresponding to the doubled perovskite are labelled with asterisks in the X-ray pattern of the x = 0.06 perovskite. Splitting of the (200) reflections are shown as insets.

peaks associated with the doubled cell, marked with arrows in Fig. 2, are broad while those of the cubic sublattice are narrower. These results are consistent with the results obtained from Ibarra et al [6]. The appearance of the superstructure peaks are due to alternate arrangement of the La^{3+}, Li^+ ions and vacancies on the adjacent ab plances along the c axis. For samples with low lithium content (x = 0.06), superstructure peaks are sharp and strong. The intensity of the superstructure peaks decrease and broadened lines as the lithium content in sample increased. Because the distribution of the La^{3+}, Li^+ ions and vacancies become more disorder when Li content in sample increases.

iii) For samples with low lithium content (x = 0.06), the XRD patterns are slightly different. Splittings of different peaks have been detected, in particular, (200) line split into three components (004), (200) and (020) (see inset of the Fig. 2), indicating the presence of an orthorhombic distortion in the perovskite network [6].

Fig. 3 shows the Raman spectra of LLTO measured at room temperature with different lithium contents ($x = 0.06$, 0.11 and 0.15). It can be seen 5 bands featured in every street, they are marked by the letters A, B, C, D and E. When not into account lithium content and heat treatment, these spectra can be explained based on the tetragonal structure of LLTO [16, 17]. Differences between obtained spectra is only the less shift of location and Raman intensities of the strips when lithium content change. These results are consistent with the results obtained from X-ray diffraction research. The structural parameters of LLTO change very small in lithium content range from $x = 0.06$ to 0.15. Small changes detected along the series have been mainly ascribed to cation disorder which increases when the lithium content increases. When the lithium content in LLTO increase, link between the oxygen atom and the lithium cation changes, have reduced the intensity of the Ti-O link. The scattering peak detection in high frequency bands (E) in the LLTO06 sample denote orthorhombic distortion in the structure [16].
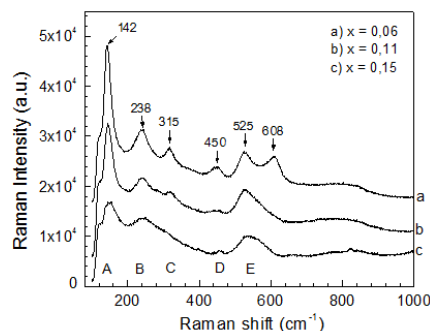
Fig. 3. Room temperature Raman spectra of $La_{(2/3-x)}Li_{3x}TiO_3$ samples with different lithium contents: a) $x = 0.06$, b) $x = 0.11$ and c) $x = 0.15$.
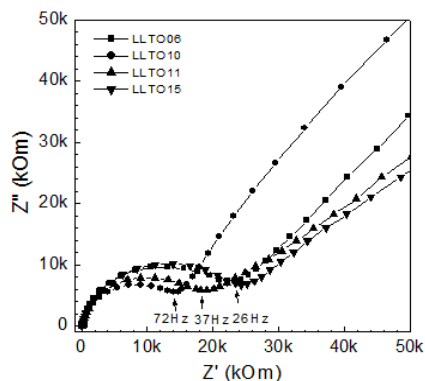
Fig. 4. Complex impedance diagrams of LLTO06, LLTO10, LLTO11 and LLTO15 samples were measured at room temperature and in the range of frequencies from 1 MHz to 0.1 Hz.

III.2. **Ionic conductivity**

Fig. 4 shows the complex impedance diagrams (CID) of the LLTO06, LLTO10, LLTO11 and LLTO15 samples at room temperatures. From this figure one can see that all the CIDs consist of two parts: the first part is the semicircle relating to grain-boundaries conductivity and the second one is the line obtained at low frequencies that relates to the diffusion process in the Helmholtz layer.

From the CIDs can be seen, the grain resistance (R_g - intercept point of the semicircle by the real axis towards high frequency) changes slightly when changing lithium content. In contrast, the grain boundary resistance (R_{gb} - intercept point of the semicircle by real axis towards low frequency) significant changes according to lithium content in sample.

For the accurate determination of the ionic conductivity we used a fitting method between experimental curves and the theoretical curves obtained from equivalent schema to the CIDs. These CIDs of the $La_{2/3-x}Li_{3x}TiO_3$ samples with Ag electrode (Ag | LLTO | Ag) were well fitted by the equivalent schema of $R_g(C_{gb}R_{gb})(R_cQ_c)(C_{in}[R_{in}(C_{dl}W)])$. By this schema, R_g is the resistance characterizing the grain conductivity; R_{gb} and C_{gb} are the resistance and capacity of grain boundaries, respectively; R_{in} and C_{in} are the resistance and the capacity formed by the contact between the Ag thin film electrode and samples surface; W and C_{dl} are the Waburg impedance characterizing the charge shift and the capacity of the double charge layer, respectively; R_c and Q_c are the resistance and the constant phase component (CPE) related to electrodes, respectively.

To determine the ionic conductivity (σ) one can use the following formula:

$$\sigma = \frac{d}{R.A}, \tag{3}$$

where, d is the thickness of the sample (d = 0.1 cm), A – area (A = 0.5 cm^2) and R– resistance relating to ionic conductance that is determined from equivalent schema.

The obtained results of the calculation for all the samples are listed in Table 1. Table 1 shows ion conductivity values measured at room temperature, as a function of lithium content in the solid LLTO solution. The maximum value of grain conductivity is obtained for lithium content of x = 0.11, namely $\sigma_g = 1.5 \times 10^{-3}$ S.cm^{-1}. Meanwhile grain boundaries conductivity reached the highest value for samples with lithium content x = 0.10, namely 5.8×10^{-5} S.cm^{-1}. These values of the conductivities are fairly larger than the one of $La_{(2/3)-x}Li_{3x}TiO_3$ sample prepared by method of conventional solid-state reactions that was reported [2-6,15,18]. This was explained by the different loss of Li ions during annealing at high temperatures. Grain conductivity increase may be due to: i) By the dMA method, LLTO compounds formed in react-grinding process at low temperatures, thereby limiting the evaporation of lithium. The compounds received had the ideal stoichiometry; ii) Samples have fabricated high uniformity.

Dependence of the ionic conductivity on ambient temperature are investigated with in-situ impedance spectroscopic measurements with temperature range from 30 to 200°C. Fig. 5 shows the Arrhenius plots of LLTO ceramics. A bending of the curve, similar to those reported in [2,6,18,19,21] has been observed. As shown in Fig. 5, one transition point in Arrhenius plots of the grain and grain-boundaries conductivities can be determined for different specimens, which relate to tilt or rotate the TiO$_6$ octahedra, leading to "open or close the bottle neck" in the perovskite structure, through which lithium ions move into nearby A-site vacancies. When the temperature

Table 1. Li-ionic conductivity vs. Li concentration in LLTO samples made by dMA method

Sample	Li^+ conductivity (S/cm)		
	σ_b /10^{-3}	σ_{gb} /10^{-5}	σ_{tp} /10^{-5}
LLTO06	1,0	3,9	3.8
LLTO09	1,2	5,0	4.8
LLTO10	1,3	5,8	5.6
LLTO11	1,5	4,5	4.4
LLTO12	1,4	4,0	3.9
LLTO13	1,2	3,5	3.4
LLTO15	1,1	3,2	3.1

increases could make the tilt and/or rotate of octahedra upwards easier, this process leads to promote ion thermal support mechanism [19,20]. The plots of $\ln(\sigma T)$ against $1000/T$ in Fig. 5 are found to follow the Arrhenius law expressed as $\sigma \sim \sigma_o/T \exp(-E_a/kT)$.

a)   b)
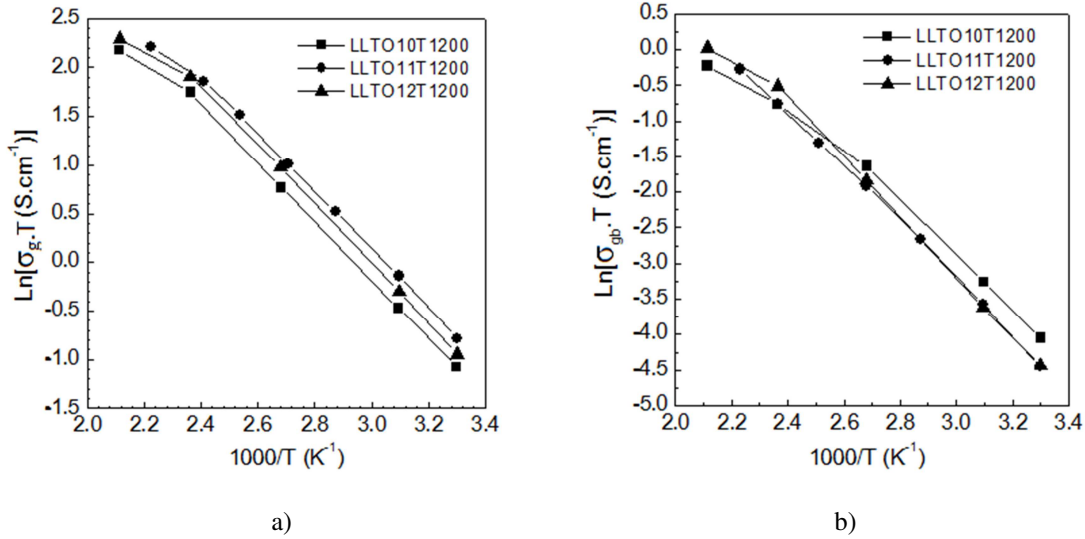
Fig. 5. Arrhenius plots of the LLTO samples: a) for grain conductivity, b) for grain-boundary conductivity.

From the Arrhenius plots, activation energy (E_a) was determined. The results showed that the activation energy for grain and grain-boundary conductivity of samples with different lithium content value not significantly different: $E_{ag} = (0.23 \pm 0.01)$ eV and $E_{agb} = (0.32 \pm 0.02)$ eV, respectively. These values ??are smaller than the activation energy obtained from the sample is made of solid state reaction (0.36 eV [2-6]).

IV. CONCLUSION

Ultrafine perovskite-type LLTO powders with an optimal Li-content (x $\sim$ 0.10) were successfully synthesized at near room temperature by solid-state reactions using the dMA method.

The dMA method appeared to be more suitable due to the mixing of elements at molecular level during the synthesis. Structural modifications are produced mainly due to cation vacancies ordering along the c-axis, which disappear gradually when the lithium content increases. The LLTO ceramics obtained when sintered at high temperature are considered pure ionic conductive materials. At room temperature, the lithium ionic grains and grain boundaries conductivities of the LLTO11 and LLTO10 have a maximum value of 1.5×10^{-3} S/cm and 5.8×10^{-5} S/cm, respectively. In all samples analysed, a non-Arrhenius temperature dependence of ionic conductivity was obtained. At temperature from 30 to 125 ^{o}C, the activation energy for grain and grain-boundary conductivity was found to be of ~ 0.23 eV and ~ 0.32 eV, respectively.

ACKNOWLEDGEMENT

REFERENCES

[1] C. M. Lampert and C. G. Granqvist, eds, in "*Large-area Chromogenics: Materials and Devices for Transmittance Control*", Vol. 154 (SPIE Optical Engineering Press, Bellingham, 1990).

[2] Y. Inaguma, C. Liquan, M. Itoh, T. Nakamura, T. Uchida, H. Ikuta, M. Wakihara, Solid State Commun. 86 (10) (1993) 689-693.

[3] Y. Inaguma, L. Chen, M. Itoh, T. Nakamura, *Solid State Ionics* **70/71** (1994) 196-202.

[4] Y. Harada, T. Ishigaki, H. Kawai, J. Kuwano, *Solid State Ionic*, **108** (1998) 407-413.

[5] A. G. Belous, *Journal of the European Ceramic Society* **21** (2001) 1797.

[6] J. Ibarra, A. Varez, C. Leon, J. Santamarіa, L. M. Torres-Martinez, J. Sanz, *Solid State Ionics* **134** (2000) 219–228.

[7] Le Dinh Trong, Nguyen Nang Dinh, Pham Duy Long, J. Mat. Sci. Eng. (A & B) (J.MSE) (2014) xxx (Accepted for publication)

[8] J.A. Alonso, J. Sanz, J. Santamaría, C. Léon, A. Várez, M.T. Fernánez-Díaz, *Angew. Chem.* **39**(2) (2000) 619.

[9] J. Sanz, J.A. Alonso, A. Várez, M.T. Fernánez-Díaz, *Journal of Solid State Chemistry* **177** (2004) 1157–1164.

[10] O. Bohnke, H. Duroy, J.L. Forquet, S. Ronchetti, D. Mazza, *Solid State Ionics* **149** (2002) 217.

[11] A. Várez, J. Ibarra, A. Rivera, C. Léon, J. Santamaría, M.A. Laguna, M.L. Sanjuán, J. Sanz, *Chem. Mater.* **15** (2003) 225.

[12] A. Rivera, C. León, J. Santamaría, A. Várez, M.A. Paris, J. Sanz, *Journal of Non-Crystalline Solids* **307–310** (2002) 992-998.

[13] T. Okumura, T. Ina, Y. Orikasa, H. Arai, Y. Uchimoto, Z. Ogumi, J. Mater. Chem. 21 (2011) 10195-10205.

[14] Y. Inaguma, T. Katsumata, M. Itoh, Y. Morii, T. Tsurui, *Solid State Ionics* **177** (2006) 3037-3044.

[15] Kai-Yun Yang, Jian-Wen Wang, Kuan-Zong Fung, Journal of Alloys and Compounds 458 (2008) 415–424.

[16] M. A. Laguna, M. L. Sanjuán, A. Várez, and J. Sanz, P*hysical review B* **66** (2002), pp. 054301-1 – 054301-7.

[17] M. L. Sanjuán and M. A. Laguna, *Physical Review B* **64** (2001) 174305-1 – 174305-5.

[18] C. W. Ban, G. M. Choi, *Solid State Ionics* **140** (2001) 285–292.

[19] O. Bohnke, C. Bohnke, J.-L. Fourquet, *Solid State Ionics* **91** (1996) 21-31.

[20] M. Vijayakumar, O. Bohnke, Journal of the European Ceramic Society 26 (2006), pp. 3221-3231.

[21] C. Leon, J. Santamaría, M. A, París, J. Sanz, J. Ibarra, L. M. Torres, *Physical Review B* **56**(9) (1997) 56-5302 - 56-5305.